A phosphorylation-dependent switch of the lysosomal V-ATPase assembly regulates α-synuclein clearance in glia

Shiping Zhang[1†], Linfang Wang[1,†], Shuanglong Yi[1,†], Shuhua Li[1], Honglei Wang[1], Ruiqi Wang[1], Yang Liu[4], Wei Yan[5], Chang Liu[5], Kai-Wen He[4], Margaret S. Ho[1,2,3,*]

[1]School of Life Science and Technology, ShanghaiTech University, Shanghai, 201210, China

[2]Institute of Neuroscience, National Yang Ming Chiao Tung University, Taipei, Taiwan

[3]Brain Research Center, National Yang Ming Chiao Tung University, Taipei, Taiwan

[4]Interdisciplinary Research Center on Biology and Chemistry, Shanghai Institute of Organic Chemistry, Chinese Academy of Sciences, Shanghai 201210, China

[5]Guangdong Provincial Key Laboratory of Brain Connectome and Behavior, CAS Key Laboratory of Brain Connectome and Manipulation, the Brain Cognition and Brain Disease Institute (BCBDI), Shenzhen Institutes of Advanced Technology, Chinese Academy of Sciences; Shenzhen-Hong Kong Institute of Brain Science-Shenzhen Fundamental Research Institutions, Shenzhen, 518055, China

[†]These authors contributed equally

*Corresponding author: Margaret S. Ho, Ph.D. Email: margareth@shanghaitech.edu.cn

Abstract

Glia serve as double-edged swords to modulate neuropathology in Parkinson's disease (PD), but how they react opposingly to be beneficial or detrimental under pathological conditions, like promote or eliminate α-synuclein (α-syn) inclusions, remains elusive. Here we present evidence that the PD risk factor Cyclin G-associated kinase (GAK)/dAuxilin (dAux) regulates the lysosomal degradation of α-syn in glia. In addition to a broad spectrum of parkinsonian symptoms in *Drosophila* and mice, lack of glial Gak/dAux causes abnormally higher α-syn levels in fly and mouse brains, and further enhances the α-syn preformed fibril levels in mouse brains. dAux phosphorylates at the serine 543 of Vha44, the V1C subunit of the vacuolar H^+-ATPase (V-ATPase), regulates the V-ATPase assembly, and controls the lysosomal acidification and hydrolase activity to set an acidic milieu for α-syn degradation in glia. Importantly, blocking Vha44 serine 543 phosphorylation disrupts V-ATPase assembly, lysosome acidification, and hydrolase activity, leading to DA neurodegeneration and locomotor deficits in flies. Our findings identify a phosphorylation-dependent switch controlling the V-ATPase assembly for lysosomal α-syn degradation in glia. Targeting the clearance of glial α-syn inclusions via this lysosomal pathway could potentially be a therapeutical approach to ameliorate the disease progression in PD.

Keywords: Parkinson's disease; Lysosomal acidification; V-ATPase; α-syn

degradation; Glia

Introduction

Protein inclusions in the brains are the histological hallmarks for neurodegenerative diseases, and a strategic way to target them for elimination is urgently needed to resolve the pathology. Whereas Lewy bodies (LBs), the fibrillar aggregates of α-synuclein (α-syn), accumulate in neurons in Parkinson's disease (PD), evident α-syn inclusions are also detected in microglia, astrocytes, and oligodendrocytes due to prion-like propagation from neurons to glia[1-4]. In addition, glia (astrocytes and microglia) are double-edged swords in PD and respond to signals from neuronally-secreted α-syn by releasing pro- or anti-inflammatory factors to enhance or ameliorate PD progression, respectively[5-10]. While it is clear that neuronal α-syn inclusions are eliminated via the autophagy-lysosome pathway, the mechanism of how α-syn inclusions are eliminated in glia remains largely elusive.

Lysosomes, the acidic milieu containing hydrolases and other enzymes, are the final destinations for endocytic and autophagic pathways to digest extracellular and intracellular materials[11-13]. To maintain an optimal pH, the vacuolar H^+-ATPase (V-ATPase) localizes on the lysosomal membrane and pumps protons into the lumen[14-16]. V-ATPase is a multisubunit enzyme composed of a cytosolic V1 domain with eight subunits (A-H) mediating ATP hydrolysis and a membrane-bound V0 domain with six subunits (a, c, c", d, e, and c' in yeast or Ac45 in higher eukaryotes) mediating proton transport[16-18]. Using the energy generated by ATP hydrolysis, V-ATPase drives the ion flux to regulate a variety of cellular processes, such as

endosome maturation and trafficking, receptor recycling, and nutrient signaling[19,20]. Notably, the function of V-ATPase in controlling lysosomal acidification could well be a key factor tuning the level of protein inclusions in the disease brains; how V-ATPase contributes to the pathological aggregate formation and elimination, awaits to be further explored.

Here we present evidence that a lysosomal pathway orchestrated by a phosphorylation-dependent switch of the V-ATPase assembly regulates α-syn degradation in glia. dAuxilin (dAux), the *Drosophila* homolog of the human Cyclin G-associated kinase (GAK, mouse Gak), regulates the serine 543 (S543) phosphorylation of Vha44, the catalytic C subunit of the V-ATPase V1 complex. Lack of dAux decreases Vha44 S543 phosphorylation, reduces V-ATPase assembly, and disrupts lysosomal acidification and hydrolase activity in glia. These defects ultimately cause α-syn accumulation, leading to a broad spectrum of parkinsonian phenotypes including DA neurodegeneration and locomotor deficits in flies and mice. Our findings identify a lysosomal α-syn clearance pathway that functions in a glial context contributing to neurodegeneration; targeting the lysosomal α-syn degradation in glia might be a strategic way to eliminate protein inclusions in PD.

Results

Lack of glial Gak/dAux causes a broad spectrum of PD-like symptoms

Our previous study indicated that GAK/dAux plays a role in autophagy initiation in

glia[21,22]. Promoting autophagy initiation, however, is in apparent contradiction to the observed block in substrate degradation in the absence of GAK/dAux, leading us to speculate whether there are additional regulations conferred by GAK/dAux. We then further investigated the pathological significance of lacking Gak/dAux, in hope to gain more mechanistic details at the cellular level. As previously reported, two independent transgenic fly RNAi lines targeting *daux*: *daux*-RNAi (V#16182) and *daux*-RNAi[#2] (BL#39017) were expressed in glia using the pan-glial *repo*-GAL4[21]. Flies expressing *UAS-LacZ* or *UAS-luciferase*-RNAi (*luc*-RNAi, Figure S1) were used as controls throughout the study. Consistent to our previous findings, lacking glial dAux in flies caused age-dependent loss of dopaminergic (DA) neurons in the PPM1/2 cluster (Figures 1A-1C, S1A and S1B, S2A and S2B), where DA neurons have been shown to degenerate upon α-syn overexpression[23]. These flies also exhibited locomotor deficits (Figures 1D, S1C, and S2C) and reduced lifespan (Figures 1E and S1D). Some of the earlier PD-associated symptoms such as sleep disturbance were also detected upon glial dAux depletion (Figures S3A and S3B). Consistently, lacking microglial Gak caused significant DA neuron loss in the conditional knockout (cKO) mice (*CX3CR1-Cre*$^{+/-}$*; Gak*$^{flox/flox}$, henceforth *Gak* cKO)[21] (Figures 1F and 1G), locomotor deficits quantified by the footprint analysis and pole test (Figures 1H and 1I), and body weight loss (Figure 1J). Taken together, Gak/dAux expression in glia contributes to a broad spectrum of PD-like symptoms including DA neurodegeneration, locomotor dysfunction, and shorten lifespan in flies and mice.

α-syn are accumulated in glial lysosomes in the absence of Gak/dAux

Importantly, upon co-expression of human α-syn in neurons and *daux*-RNAi in glia using a GAL4/lexA binary system, total α-syn levels in the brains increased in the absence of glial dAux (Figures 2A and 2B). α-syn proteins were also detected in the sorted wild type fly glia, despite its neuronal origin (Figure S3C). These results indicate that α-syn transmits from neurons to glia and accumulates in the absence of glial dAux.

Furthermore, whereas *Gak* cKO microglia exhibited shorter processes, higher CD68-positive phagocytic activity, and amoeboid-like structures in a potentially activated state (Figures 2C-E), phosphorylated α-syn levels detected by the antibodies against the phosphorylated serine 129 (pS129-α-syn) and its colocalization with the microglia marker ionized calcium-binding adapter molecule 1 (Iba1) were also elevated in *Gak* cKO microglia (Figures 2F and 2G). Upon the bilateral inoculation of the α-syn preformed fibril (PFF) in the dorsal striatum, microglial pS129-α-syn intensities and pS129-α-syn-Iba1 colocalization increased in the substantia nigra (SN) (+/- PFF, Figures 2H-2J), and further increased in the PFF-treated *Gak* cKO mice compared to the Cre alone controls, indicating that lacking microglial Gak promotes pS129-α-syn accumulation (Figures 2I and 2J). These results demonstrate that Gak/dAux regulates the degradation of pathological α-syn inclusions in glia.

By a closer look, the accumulated α-syn in adult fly brains were enriched in glial

lysosomes as both the α-syn intensities inside the Lamp1-positive lysosomes and α-syn-Lamp1 colocalization increased upon *daux*-RNAi expression in glia (Figures 2K and 2L). Consistently, pS129-α-syn were also highly colocalized with lysosomes in the *Gak* cKO microglia (Figures 2M and 2N). These results implicate a lysosomal pathway orchestrated by Gak/dAux for degrading pathological α-syn in glia.

Lack of Gak/dAux increases lysosome biogenesis and disrupts lysosomal acidification in glia

To further dissect the role of Gak/dAux in lysosomal α-syn degradation, Lamp1-GFP was co-expressed to label glial lysosomes. Upon *daux*-RNAi expression, the number of glial Lamp1-positive lysosomes increased in the brains (Figures 3A and 3B). Consistent to observations in previous studies[24-26], some of these lysosomes were enlarged and clustered, implying non-degraded substrate accumulation (Figures 3A and 3B, S1E and S1F, S2D and S2E). Moreover, the lysosomal intensities in both the immortalized microglia (IMG) treated with siRNAs targeting *Gak* (*Gak* siRNA$^{\#1}$ and *Gak* siRNA$^{\#2}$) and *Gak* cKO microglia were elevated (Figures 3C-3F). The Lamp1-positive puncta size and the Lamp1-Iba1 colocalization in these microglia were also increased (Figures 3E and 3F). These results suggest conserved function of Gak/dAux on lysosome biogenesis. Next, ultrastructural analysis by Transmission Electron Microscopy (TEM) also revealed an increase in the lysosome number and size in the absence of glial dAux (Figures 3G and 3H, yellow arrowheads). Notably,

some of the large lysosomes were with electron-lucent dots inside or decreased intensity (Figures 3G and 3H, red or blue arrowheads, respectively), suggesting disrupted lysosomal pH[27,28].

To further probe lysosomal pH, Lysotracker Green (LTG), a fluorescent dye that specifically labels acidic organelles including the lysosomes, was used. The number and intensities of LTG-positive puncta were significantly reduced in flies lacking glial dAux, indicating that lysosomes are not properly acidified (Figures 3I and 3J, S1G and S1H, S2F and S2G). In addition, the activity of the lysosomal hydrolase Cathepsin B (CTSB) stained by Magic Red (MR) was significantly decreased (Figures 3K and 3L, S1I and S1J, S2H and S2I), and the processing of CTSB and another lysosome hydrolase Cathepsin D (CTSD) was also impaired (Figures 3M-3P). In the scale of a single glial lysosome, the mean intensities of Lysotracker Red (LTR) or MR per Lamp1-positive lysosome also decreased significantly upon dAux depletion (Figures 3Q-3T, S1K-S1N, S2J and S2K). It is noteworthy to mention that the expression of either fly dAux or human GAK (Flag-hGAK)[21] fully rescued the *daux*-RNAi-induced lysosomal acidification defects (Figures S4A and S4B), suggesting conserved GAK/dAux function on lysosome acidification. As a consequence, autophagic substrates Ref(2)P (the *Drosophila* ortholog of P62) and Ubiquitin (Ubi) accumulated in these defective lysosomes (Figures 3U and 3V, S1O and S1P, S2L and S2M). In summary, lack of glial dAux disrupts lysosomal acidification and hydrolase activity, leading to impaired substrate degradation.

dAux regulates Vha44 S543 phosphorylation

Previous studies have revealed an impact on lysosome homeostasis using GAK kinase inhibitors[24,25]. However, whether Gak/dAux regulates lysosome biogenesis and acidification via its kinase activity remains largely unexplored. To this end, phosphoproteomic analysis was conducted using adult fly head samples from the control and *repo>daux*-RNAi flies[21] (Figures S4C-G). Interestingly, a list of proteins encoding different subunits of the lysosomal V-ATPase were identified (Figures 4A-4D). As V-ATPase is the main driving force to maintain lysosomal pH, we paid special attention to the phosphorylation profiles of these subunits. Among all, the phosphorylation level at the S543 of the V-ATPase V1C subunit, Vha44 isoform F, was significantly decreased upon glial dAux depletion (*daux*-RNAi/LacZ ratio 0.634, Figure 4D). Motif analysis also predicted that S543 belongs to a sequence motif prone to be phosphorylated (xxxxPx_S_Pxxxxx, Figure 4E). These results suggest that Vha44 is likely a dAux kinase substrate.

To support our hypothesis, co-immunoprecipitation (Co-IP) analysis was first conducted. Our results revealed that dAux interacts with Vha44 both endogenously and upon overexpression in S2 cells (Figures 4F and 4G). In addition, antibodies that specifically recognize the synthesized phosphopeptides EFPL(S-p)PAEL, sequence correlating with the identified motif, were raised (anti-pVha44^{S543}). Dot blot analysis validated the specificity of anti-pVha44^{S543} antibodies to the phosphopeptide

immunogen (Figure 4H). Consistent to results from the phosphoproteomic analysis, endogenous Vha44 S543 phosphorylation probed by the anti-pVha44^{S543} antibodies was significantly reduced in adult fly brains expressing the *daux*-RNAi in glia (Figures 4I and 4J). These results suggest that dAux phosphorylates Vha44 at S543. Of note, expression of the dAux variant lacking the kinase domain (Flag-dAux$^{\Delta Kinase}$) failed to restore the *daux*-RNAi-induced lysosomal acidification defects, reinforcing the importance of the dAux kinase activity (Figures S4A and S4B).

Vha44 S543 phosphorylation regulates lysosomal acidification in glia

Next, we investigated if Vha44 S543 phosphorylation, like dAux, regulates lysosome acidification in glia. Consistent to the results from *daux*-RNAi-expressing flies, glial expression of *vha44*-RNAi, which efficiency was validated by qRT-PCR and WB analyses (Figures S5A-S5C), caused a reduction in the number of LTG- and MR-positive puncta in adult fly brains (Figures 5A and 5B, S5D and S5E). The intensities of the LTG- or LTR-positive puncta in the brains or per glial Lamp1-positive lysosome, respectively also decreased significantly upon dAux depletion (Figures 5A and 5B, 5E, and 5F). These results demonstrate that Vha44 regulates lysosomal acidification in glia.

Next, transgenic flies were made to express the wild type Vha44 (Myc-Vha44) or the non-phosphorylatable Vha44 mutant with alanine substitution of S543 (Myc-Vha44^{S543A}). These Vha44 variants were expressed properly as validated by

WB (Figure S5F). Notably, glial expression of Myc-Vha44^{S543A}, but not Myc-Vha44, caused a significant reduction on the number and intensities of the LTG-positive puncta in the adult fly brains (Figures 5C and 5D). In addition, the mean LTR intensities per Lamp1-positive lysosome were also reduced upon Myc-Vha44^{S543A} expression in glia (Figures 5G and 5H). On the other hand, glial expression of either Myc-Vha44 or Myc-Vha44^{S543A} reduced the intensities of the MR-positive puncta in the brains, with the latter exhibited a more potent suppression (Figures S5G and S5H). Taken together, Vha44 S543 phosphorylation regulates lysosomal acidification in glia.

dAux regulates lysosomal acidification and hydrolase activity via Vha44 S543 phosphorylation in glia

Given that both dAux and the Vha44 S543 phosphorylation are involved in regulating lysosomal acidification in glia, we next tested if altering the Vha44 S543 phosphorylation affects the *daux*-RNAi-induced lysosomal defects. By epistatic genetic analysis, Myc-Vha44 expression in the presence of *daux*-RNAi significantly rescued the decrease in the number and intensities of LTG- or MR-positive puncta in the whole brains or per glial Lamp1-positive lysosome, respectively, whereas the Myc-Vha44^{S543A} expression in glia failed to restore such decrease (Figures 5I and 5J, and S5I-S5N). These results further demonstrate that dAux regulates lysosomal acidification and hydrolase activity via Vha44 S543 phosphorylation in glia.

dAux-mediated Vha44 S543 phosphorylation regulates V-ATPase assembly in glia

V-ATPase is the key factor controlling lysosomal pH by pumping protons into the lumen. As we are seeing consistent phenotypes on lysosomal acidification, we next asked if the V-ATPase function, mainly relying on its V1-V0 subcomplex assembly, is regulated by the Vha44 S543 phosphorylation. Transgenic flies that express EGFP-Vha44 labeling the V1C subunit and mCherry-Vha100-2 labeling the V0a subunit were made to analyze the fluorescent signal colocalization of these two subunits, an indicator of how well the V-ATPase assembles (Figure 6A). As EGFP-Vha44 expression in glia revealed signals mainly distributed on the glial processes, mCherry-Vha100-2 expression in glia exhibited as puncta, localizing on the lysosomal membrane (Figure 6). The EGFP-mCherry co-positive signals represent how well the two subunits colocalize, providing insights into the V-ATPase assembly process. Interestingly, EGFP-mCherry co-positive signals decreased significantly upon glial dAux depletion (Figures 6B and 6C). Using the mCherry-Lamp1 as a different reporter, the EGFP-mCherry co-positive signals representing the Vha44 colocalization with Lamp1 also decreased significantly (Figures 6D and 6E). In addition, live-cell imaging analysis showed that the percentage of EGFP-positive puncta (Vha44) being trafficked to the vicinity of mCherry-positive puncta (Vha100-2, within a radius of 0.38 um) decreased (Figures 6F and 6G) and the duration time of the Vha44-Vha100-2 contact was shorter (Figures 6F and 6H) upon glial dAux

depletion. The trafficking speed of EGFP- and mCherry-positive puncta increased and remain unaffected, respectively in the absence of glial dAux, suggesting that Vha44 is more mobile (Figures 6F and 6I). Altogether, these results demonstrate that glial dAux regulates the V-ATPase assembly.

To analyze whether Vha44 S543 phosphorylation affects the V-ATPase assembly, transgenic flies expressing the EGFP-Vha44^{S543A} variant carrying the alanine substitution of S543 were made. Compared to EGFP-Vha44, EGFP-Vha44^{S543A} expression in glia reduced the Vha44^{S543A} colocalization with Vha100-2 or Lamp1, suggesting that Vha44 S543 phosphorylation is crucial for the V-ATPase assembly (Figures 6B-6E). Whereas *daux*-RNAi expression in glia reduced Vha44 colocalization with Vha100-2 or Lamp1, it failed to impact on the Vha44^{S543A} colocalization with either, suggesting that dAux mediates V-ATPase assembly via Vha44 S543 phosphorylation (Figures 6B-6E). Accordingly, it is noteworthy to mention that Manders' Correlation was carefully chosen to analyze the colocalization of EGFP-Vha44 or EGFP-Vha44^{S543A} with Vha100-2 or Lamp1 as EGFP levels were affected by dAux (Figures 6C and 6E)[29-32].

dAux-mediated Vha44 S543 phosphorylation contributes to DA neurodegeneration and locomotor function

Given that lack of Gak/dAux leads to a broad spectrum of PD-like symptoms, we next investigated if Vha44 and its S543 phosphorylation are also regulators of these

parkinsonian phenotypes. The number of DA neurons in the PPM1/2 cluster were significantly reduced in flies lacking Vha44 or expressing Myc-Vha44^{S543A} in glia in an age-dependent manner (Figures 7A-7D). Myc-Vha44 expression in glia caused an increase in the DA neuron number at day 3, but not day 10 or 20 (Figures 7C and 7D). Furthermore, glial expression of Myc-Vha44, but not Myc-Vha44^{S543A}, restored the *daux*-RNAi-induced DA neuron loss (Figures 7E and 7F). On the other hand, *vha44*-RNAi or Myc-Vha44^{S543A} expression in glia disrupted fly locomotion in an age-dependent manner, whereas Myc-Vha44 expression in glia affects fly locomotion in various time points less potently than Myc-Vha44^{S543A} (Figures 7G and 7H). Re-introducing Myc-Vha44 expression in glia significantly rescued the *daux*-RNAi-induced locomotor deficits, whereas Myc-Vha44^{S543A} did so less potently (Figure 7I). Altogether, these results suggest that dAux-mediated Vha44 S543 phosphorylation underlies the mechanism of DA neurodegeneration and locomotor function in PD.

Discussion

Although neurodegeneration is the pathological hallmark for neurodegenerative diseases, glial responses that constitute of neuroimmune activation and signaling crosstalk during different stages have also been shown to widely contribute to the disease pathology. Furthermore, the intriguing phenomenon of protein inclusions observed in both neurons and glia raises substantial interest on how these pathological

aggregates are formed, transmitted, and eliminated in different cell types. Our findings in flies and mice demonstrate that α-syn is degraded via a lysosomal pathway in glia; alternation in the lysosome environment/acidification impairs α-syn clearance. This disruption in lysosomal pH is caused by a phosphorylation-dependent regulation on the V-ATPase assembly, controlling the pumping of protons into the lysosomal lumen to construct the acidic milieu for substrate degradation. The PD risk factor, Gak/dAux, plays a critical role in such regulation. Phenotypically, the lack of Gak/dAux causes endogenous and PFF-injected α-syn accumulation in glia, owing to the lack of phosphorylation on the serine 543 of the catalytic V1C subunit of the lysosomal V-ATPase, Vha44. The V-ATPase assembly is therefore hindered, disrupting the lysosomal pH for α-syn degradation (Figure 8).

V-ATPase subunit phosphorylation, assembly, and its pathological implication

The V-ATPase activity is modulated by the reversible association/dissociation of V1 and V0 subcomplexes in response to various conditions, such as glucose[33], amino acid[34], feeding[35], serotonin (5-hydroxytryptamine, 5-HT)[36], and cell maturation[37]. Previous reports have shown that some of the V-ATPase subunits are targets for phosphorylation. For instance, AP2 interacts and phosphorylates the V1B subunit[38]; PKA or AMP-activated protein kinase (AMPK) phosphorylates the V1A subunit[39,40]; *Arabidopsis* AtWNK8 phosphorylates the V1C subunit at multiple sites[41]. Nonetheless, how these modifications on different V-ATPase subunits impact on its

activity and function remains largely unknown. While some of the subunits are phosphorylated in isolation, some might require to be part of the complex allowing phosphorylation occurs[40,42]. Our present study uncovers a phosphorylation-dependent switch of the V-ATPase assembly, linking the subunit phosphorylation with the activity of the whole enzyme; blocking Vha44 S543 phosphorylation faithfully disrupts V-ATPase assembly.

Dysregulation of V-ATPase activity has been shown in many neurodegenerative disorders including PD[19,43]. For instance, the modification, protein level, or protein-protein interaction of the V0a1 subunit is critical for the pathology of different types of neurodegenerative diseases[44-47]. The PD risk factor leucine-rich repeat kinase 2 (LRRK2) also regulates V0a1 protein level and localization[45]. Interestingly, our current findings reveal a critical role of the V1C subunit in PD. Lack of Vha44 or blocking Vha44 S543 phosphorylation causes impaired lysosomal acidification and hydrolase activity, constituting unfavorable venues for α-syn degradation. Furthermore, flies exhibit DA neurodegeneration and locomotor deficits in the absence of Vha44 or its S543 phosphorylation. These findings indicate that wrongly modified V-ATPase subunit hinders its proper assembly and impairs lysosomal acidification, leading to potential α-syn accumulation and ultimately PD-like symptoms.

Gak/dAux: a kinase regulating lysosomal function associated with α-syn

degradation in PD

Targeting protein aggregates and inclusions in the degenerative brains has been considered as a strategic means for ameliorating disease progression. Our findings uncover the mechanism of a potential PD risk factor regulating α-syn clearance in glia. Despite that *GAK* functions in PD remains unclear, multiple SNPs have been identified in the locus containing *GAK*[48-50], implicating its clinical relevance. We identified the *Drosophila* GAK homolog, dAux, functioning as a kinase in phosphorylating Vha44 S543. In the absence of dAux, Vha44 S543 phosphorylation is significantly reduced. Considering the V-ATPase disassembly, lysosomal defects, and brain α-syn accumulation observed in the absence of glial dAux, the mechanism of dAux-mediated Vha44 S543 phosphorylation likely constitutes a lysosomal pathway associated with α-syn clearance in glia. Notably, glial expression of the dAux lacking the kinase domain causes DA neuron loss and fly locomotor deficits, and fails to rescue both in the absence of dAux (Figure S6). These parkinsonian phenotypes further link our newly identified pathway to PD. Of note, GAK interacts with LRRK2[51], yet these two proteins modulate the V-ATPase activity via different subunits: LRRK2 interacts with V0a1 whereas dAux interacts with V1C, potentiating different V-ATPase-mediated mechanisms underlying PD.

A glia-specific lysosomal pathway contributes to PD

While most of the hypotheses that underlie PD pathology are often driven by a

neuronal origin of dysfunctional machineries or cellular defects, glia have only recently drawing more attention as possible drivers for neurodegeneration[7]. For instance, the AD risk factor gene *Apolipoprotein E* (*APOE*) is predominantly expressed in astrocytes[52] and its genetic mutations are associated with an increasing risk of developing AD, supporting a role for genetic causes from glia driving neurodegeneration. Many PD risk genes, like *LRRK2*, *atg9*, and *vps13*, are also expressed in glia, and modulate neurodegeneration and α-syn accumulation in a non-cell-autonomous manner[53-56]. Our findings implicate another potential PD risk factor functioning in a glial context. Lack of glial Gak/dAux leads to a broad spectrum of parkinsonian symptoms in both flies and mice, including DA neurodegeneration, dysfunctional locomotor activity, shorten lifespan, microglial activation, and some of the earlier symptoms such as sleep defects. Consistently, DA neurodegeneration and locomotor deficits are also detected in the absence of glial Vha44. Glial expression of Vha44, but not the non-phosphorylatable Vha44 variant, restores these parkinsonian deficits. In combination with our cellular observations, these behavioral deficits together demonstrate a kinase-dependent lysosomal pathway regulating the parkinsonian symptoms in PD. Interestingly, lysosomal acidification remain largely intact upon neuronal dAux inhibition, further demonstrating the specificity of this lysosomal pathway (Figure S7).

The present study identifies a glia-specific pathway for the lysosomal degradation of α-syn. Our findings unravel the underlying mechanism of PD by uncovering a

cell-type specific clearance program for the brain α-syn inclusions. With accumulating evidence demonstrating the importance of glia in neurodegenerative diseases, these findings will help to pinpoint potential therapeutical targets from a glial perspective to ameliorate PD.

Acknowledgements

We thank Bloomington *Drosophila* Stock Center, Vienna *Drosophila* RNAi Center, the Core Facility of *Drosophila* Resource and Technology, Shanghai Institute of Biochemistry and Cell Biology, Chinese Academy of Sciences, and Aike Guo for fly stocks; Chih-Hao Lee for IMG cell line; Jiawei Zhou for *CX3CR1-Cre* mice. We also thank the Molecular Imaging Core Facility (MICF), the Molecular and Cell Biology Core Facility (MCBCF), and the Multi-Omics Core Facility (MOCF) at the School of Life Science and Technology, ShanghaiTech University for providing technical support; Cong Liu for helping with PFF synthesis; Yu Kong and Lijun Pan in Electron Microscopy Facilities of Center for Excellence in Brain Science and Technology, Chinese Academy of Science for assistance with TEM sample preparation; Ho lab members for discussion and comments. This work was supported by grants from ShanghaiTech, National Natural Science Foundation of China (32170962, 32271004, 32371063, and 32071009), and 2030 Cross-Generation International Outstanding Young Scholars Program (National Science and Technology Council Taiwan).

Author contributions

S.Z, L.W, S.Y, and M.S.H conceived and designed the study. S.Z, L.W, S.Y, S.L, H.W, R.W, Y.L, and W.Y performed the experiments. S.Z, L.W, S.Y, C.L, K.W.H, and M.S.H analyzed the data. S.Z, L.W, S.Y, and M.S.H wrote the paper. All authors read and approved the manuscript.

Declaration of Interests

The authors declare no competing interests.

Figure Legends

Figure 1. Glial Gak/dAux contributes to a broad spectrum of PD-like symptoms

(**A**) Illustration of an adult fly brain with different DA neuron clusters. The selected areas in red dotted rectangle identify PPM1/2 clusters and are enlarged in B. The adult brain for imaging is positioned with coordinates described (A: Anterior, P: Posterior, M: Medial, L: Lateral, D: Dorsal, V: Ventral). (**B** and **C**) Representative images (B) and quantifications (C) of DA neuron number in the control and *UAS-daux*-RNAi; *repo*-GAL4 (*repo>daux*-RNAi) adult fly brains. Note that DA neuron number in the PPM1/2 cluster decreases in an age-dependent manner upon glial dAux depletion. At 2 hours after eclosion, the DA neuron number remains similar, ruling out the developmental defects. (**D** and **E**) Locomotor function and lifespan of both male and female flies are disrupted upon glial dAux depletion. (**F** and **G**) The number of DA neurons marked by the anti-TH antibodies in the substantia nigra (SN) decreases in microglial *Gak* cKO (*CX3CR1-Cre*$^{+/-}$*; Gak*$^{flox/flox}$) mice at 36 weeks. (**H-J**) Footprint analysis, pole test and the body weight of the microglial *Gak* cKO mice. Note that

these mice exhibit locomotor deficits and weight lighter at 21 and 36 weeks. Scale bars and the sample number present as scatter dots are indicated in the Figures. A serial confocal Z-stack sections were acquired at the similar plane of brains across all genotypes, with representative images shown as maximal projection. Data are shown as mean ± SEM. P-values of significance (indicated with asterisks, ns no significance, * $p<0.05$, ** $p<0.01$, *** $p<0.001$, and **** $p<0.0001$) are calculated by two-tailed unpaired t-test, Mann Whitney test, ordinary one-way ANOVA followed by Tukey's multiple comparisons test, or Kruskal-Wallis tests followed by Dunn's multiple comparisons test.

Figure 2. Lack of Gak/dAux causes α-syn accumulation in the glial lysosomes (**A** and **B**) Representative images (A) and quantifications (B) of α-syn intensities (Myc-positive, green) in adult fly brains expressing *daux*-RNAi in glia and *SNCA* in neurons using a GAL4/lexA binary system (*UAS-daux*-RNAi; *repo*-GAL4, *UAS-mCD8-RFP*, *GMR57C10*-lexA, *lexAop-6xMyc-SNCA*). *UAS-mCD8-RFP* is co-expressed by *repo*-GAL4 to label glial processes (red). Note that total α-syn intensities significantly increase upon glial dAux depletion. (**C-E**) Representative images (C) and quantifications (D and E) of *Gak*-deficient microglia. Both the intensity of CD68 (a macrophage marker indicating the phagocytic activity of microglia, green) in Iba1-positive microglia (red) and the CD68-Iba1 colocalization increase when lacking microglial *Gak*. 3D reconstruction reveals activated microglia with shorter branches, fewer terminal points, and larger cell bodies upon Gak depletion. (**F** and **G**) Representative images (F) and quantifications (G) of pathological α-syn phosphorylated on S129 (pS129-α-syn, green) in Iba1-positive microglia (red). Note that both pS129-α-syn intensities in Iba1-positive microglia and

pS129-α-syn-Iba1 colocalization increase in *Gak*-deficient microglia. (**H**) Illustration of mouse brains bilaterally inoculated with the α-syn preformed fibril (PFF) in the dorsal striatum. (**I** and **J**) Representative images (I) and quantifications (J) of pathological α-syn in mouse brains injected with α-syn preformed fibril (PFF). Note that both pS129-α-syn intensities in Iba1-positive microglia and the pS129-α-syn-Iba1 colocalization increase in PFF-treated mouse brains. Lacking microglial Gak further enhances both. (**K and L**) Representative images (K) and quantifications (L) of lysosomal α-syn intensities in adult fly brains expressing *mCherry-Lamp1* and *daux*-RNAi in glia and *SNCA* in neurons (*UAS-mCherry-Lamp1*, *UAS-daux*-RNAi; *repo*-GAL4, *GMR57C10*-lexA, *lexAop-6xMyc-SNCA*). Note both the α-syn intensities in Lamp1-positive lysosomes and α-syn-Lamp1 colocalization increase upon glial dAux depletion. (**M and N**) The pS129-α-syn-Lamp1 colocalization in mouse SN microglia increases upon microglial Gak depletion. Scale bars and the sample number present as scatter dots are indicated in the Figures. A serial confocal Z-stack sections were taken at the similar plane of brains across all genotypes, with representative images shown as single layer or maximal projection. Colocalization is analyzed using the Pearson's Correlation and present as the Pearson's R value. Quantification Figures from the same images but with different parameters are shown under the same label unless noted otherwise. Data are shown as mean ± SEM. P-values of significance (indicated with asterisks, ns no significance, * $p<0.05$, ** $p<0.01$, *** $p<0.001$, and **** $p<0.0001$) are calculated by two-tailed unpaired t-test, Mann Whitney test, or Kruskal-Wallis tests followed by Dunn's multiple comparisons test.

Figure 3. Lack of Gak/dAux increases lysosome biogenesis and disrupts

lysosomal acidification in glia (**A**-**F**) Representative images (A, A', C, and E) and quantifications (B, D, and F) of glial lysosomes in adult fly brains (A , A', and B), IMG cells (C and D), and mouse SN microglia (E and F). Glial lysosomes (green) are marked by Lamp1-GFP in fly glia (*UAS-Lamp1-GFP; repo*-GAL4) and anti-Lamp1 antibodies in IMG cells and mouse microglia. The selected areas in white dotted squares in A are enlarged aligning on the right (A'). Note that Lamp1-positive lysosome number (B), intensities (D and F), size (F), and Lamp1-Iba1 colocalization (F) increase upon dAux or Gak depletion by *daux*-RNAi (A, A', and B), *Gak* siRNAs (C and D), or in the *Gak* cKO mice at 36 weeks (E and F). (**G** and **H**) Representative TEM images (G and G') and quantifications (H) of lysosomes in control and *repo>daux*-RNAi adult fly brains. The selected areas in white dotted squares in G are enlarged aligning on the right (G'). Note that the number and size of lysosomes (yellow arrows) increase when *daux*-RNAi is expressed in glia, and some large lysosomes exhibit electron-lucent dots inside (red arrows) or decreased intensity (blue arrow). (**I**-**L**) Representative images (I and K) and quantifications (J and L) of Lysotracker Green (LTG) and Magic Red (MR) staining in adult fly brains. Note that both number and intensities of LTG- and MR-positive puncta decrease upon glial dAux depletion. (**M**-**P**) The processing of the lysosomal proteases CTSB and CTSD were analyzed by WB analysis. Note that lacking glial dAux decreases the mature/total CTSB or CTSD ratio. (**Q**-**T**) Representative images (Q, Q', S, and S') and quantifications (R and T) of glial lysosomes (Lamp1-GFP, green) staining with Lysotracker Red (LTR, Q, Q', and R) or MR (S, S', and T) in adult fly brains. Note that LTR- or MR-positive intensities in glial lysosomes decrease. The selected areas in white dotted squares in Q and S are enlarged aligning on the right (Q' and S'). (**U** and **V**) Representative images (U) and quantifications (V) of Ubiquitin (Ubi) and Ref(2)P

levels in adult fly brains expressing *daux*-RNAi. Note that both the intensities of Ubi and Ref(2)P and the colocalization of Ubi-Lamp1 and Ref(2)P-Lamp1 increase upon glial dAux depletion. Scale bars and the sample number present as scatter dots are indicated in the Figures. A serial confocal Z-stack sections were taken at the similar plane across all genotypes, with representative images shown as single layer or maximal projection. Colocalization is analyzed using the Pearson's Correlation and present as the Pearson's R value. Quantification Figures from the same images but with different parameters are shown under the same label unless noted otherwise. Data are shown as mean ± SEM. P-values of significance (indicated with asterisks, ns no significance, * $p<0.05$, ** $p<0.01$, *** $p<0.001$, and **** $p<0.0001$) are calculated by two-tailed unpaired t-test, Mann Whitney test, or ordinary one-way ANOVA followed by Tukey's multiple comparisons test.

Figure 4. dAux regulates Vha44 S543 phosphorylation (**A**) Illustration of the V-ATPase structure. Note that V-ATPase is assembled from the V1 and V0 subcomplexes, and Vha44 is the V1C subunit. (**B**) Advanced volcano plot drawn with the phosphoproteomic data by the OmicStudio tools. The variance threshold is larger than 1.5 or less than 0.5, while the p-value is less than 0.05. Samples were collected from control or *repo>daux*-RNAi adult fly brains. (**C** and **D**) The V-ATPase subunit Vha44 phosphorylation at serine 543 is greatly reduced upon glial dAux depletion as shown by the heatmap (C) and the table listing all the affected V-ATPase subunits (D). (**E**) The sequences near S543 site of Vha44 belongs to a phosphorylation motif xxxxPx_S_Pxxxxx identified by the MoMo analysis tool using the motif-x algorithm. The motif consists of 6 amino acids upstream and downstream of the potential dAux modification site. Preferred amino acids are indicated with larger font, while less

preferred amino acids are indicated with smaller font. (**F**) Co-IP analysis using fly S2 cells reveals that endogenous dAux interacts with Vha44, detected by the anti-dAux and mammalian anti-ATP6V1C1 antibodies, respectively. (**G**) S2 cell lysates expressing Flag-dAux and EGFP-Vha44 were pulled down by beads conjugated to anti-Flag or anti-EGFP antibodies. Note that dAux and Vha44 are within the same complex by both pull downs. (**H**) Dot blot analysis revealed that the anti-pVha44^{S543} antibodies only recognized the phosphopeptide immunogen, but not the nonphosphopeptide immunogen, proving the specificity of the pVha44^{S543} antibodies. (**I** and **J**) Representative images (I) and quantifications (J) of Vha44 S543 phosphorylation. The anti-pVha44^{S543} antibodies specifically detect the phosphorylation status on Vha44 S543. Note that Vha44 S543 phosphorylation levels are reduced after normalization (pVha44^{S543}/ATP6V1C1) upon glial dAux depletion. Sample number present as scatter dots are indicated in the Figures. Data are shown as mean ± SEM. P-values of significance (indicated with asterisks, ns no significance, * $p<0.05$, ** $p<0.01$, *** $p<0.001$, and **** $p<0.0001$) are calculated by two-tailed unpaired t-test.

Figure 5. dAux-mediated Vha44 S543 phosphorylation regulates lysosome acidity in glia (**A**-**D**) Representative images (A and C) and quantification (B and D) of LTG-positive puncta in adult fly brains expressing *vha44*-RNAi, Myc-Vha44, and Myc-Vha44^{S543A}. Note that the number and intensities of LTG-positive puncta decrease upon *vha44*-RNAi or Myc-Vha44^{S543A} expression. (**E**-**J**) Representative images (E, E', G, G', I, and I') and quantifications (F, H, and J) of glial lysosomes (Lamp1-GFP, green) stained with LTR in adult fly brains. Note that the LTR intensities in the Lamp1-positive lysosomes are reduced when expressing

vha44-RNAi or Myc-Vha44^{S543A} in glia. Expression of Myc-Vha44, but not Myc-Vha44^{S543A}, rescues the *daux*-RNAi-induced decrease in the LTR intensities. The selected areas in white dotted squares in E, G, and I are enlarged aligning on the right (E', G', and I'). Scale bars and the sample number present as scatter dots are indicated in the Figures. A serial confocal Z-stack sections were taken at the similar plane of brains across all genotypes, with representative single layer images shown. Quantification Figures from the same images but with different parameters are shown under the same label unless noted otherwise. Data are shown as mean ± SEM. P-values of significance (indicated with asterisks, ns no significance, * $p<0.05$, ** $p<0.01$, *** $p<0.001$, and **** $p<0.0001$) are calculated by two-tailed unpaired t-test, Mann Whitney test, ordinary one-way ANOVA followed by Tukey's multiple comparisons test, or Kruskal-Wallis tests followed by Dunn's multiple comparisons test.

Figure 6. dAux-mediated Vha44 S543 phosphorylation regulates V-ATPase assembly in glia (**A**) Illustration of the V-ATPase structure, highlighting the subunits Vha44 tagged with EGFP (green) and Vha100-2 tagged with mCherry (red). (**B-E**) Representative images (B, B', D, and D') and quantifications (C and E) of the Vha44-Vha100-2 or Vha44-Lamp1 colocalization in adult fly brains. Note that both types of colocalization decrease upon *daux*-RNAi expression in glia. Compared to EGFP-Vha44, EGFP-Vha44^{S543A} expression reduces the colocalizations. Unlike EGFP-Vha44, the colocalizations of EGFP-Vha44^{S543A} is not altered by co-expression of *daux*-RNAi. (**F-I**) Live-cell imaging (F) and quantifications (G-I) of Vha44 trafficking to Vha100-2 in adult fly brains. Note that upon glial dAux depletion, the percentage of Vha44-positive puncta being trafficked to the vicinity of

Vha100-2-positive puncta (with a radius of 0.38 um) decreases (G), and the duration time of the Vha44-Vha100-2 contact is shorter (H). The trafficking speed of Vha44-positive puncta increases while Vha100-2-positive puncta remains unaffected (I). Scale bars and the sample number present as scatter dots are indicated in the Figures. A serial confocal Z-stack sections were taken at the similar plane of brains across all genotypes, with representative single layer images shown. Colocalization is analyzed by Manders' Correlation, taking into account the change in the protein level. Quantification Figures from the same images but with different parameters are shown under the same label unless noted otherwise. Data are shown as mean ± SEM. P-values of significance (indicated with asterisks, ns no significance, * $p<0.05$, ** $p<0.01$, *** $p<0.001$, and **** $p<0.0001$) are calculated by two-tailed unpaired t-test, Mann Whitney test, ordinary one-way ANOVA followed by Tukey's multiple comparisons test, or Kruskal-Wallis tests followed by Dunn's multiple comparisons test.

Figure 7. dAux-mediated Vha44 S543 phosphorylation contributes to DA neurodegeneration and locomotor function (**A-F**) Representative images (A, C, and E) and quantifications (B, D, and F) of DA neuron number in the adult fly brains with the indicated genotypes. Note that DA neuron number in the PPM1/2 cluster decreases in an age-dependent manner upon expressing *vha44*-RNAi or Myc-Vha44^{S543A} in glia. Myc-Vha44, but not Myc-Vha44^{S543A}, rescues the *daux*-RNAi-induced decrease in the DA neuron number. (**G-I**) Analysis of fly locomotor function in both males and females. Note that *vha44*-RNAi or Myc-Vha44^{S543A} expression in glia induces significant decline of climbing distance. Myc-Vha44, but not Myc-Vha44^{S543A}, expression in glia rescues the

daux-RNAi-induced locomotor deficits. Scale bars and the sample number present as scatter dots are indicated in the Figures. A serial confocal Z-stack sections were taken at the similar plane of brains across all genotypes, with representative shown as maximal projection. Quantification Figures from the same images but with different parameters are shown under the same label unless noted otherwise. Data are shown as mean ± SEM. P-values of significance (indicated with asterisks, ns no significance, * $p<0.05$, ** $p<0.01$, *** $p<0.001$, and **** $p<0.0001$) are calculated by two-tailed unpaired t-test, Mann Whitney test, ordinary one-way ANOVA followed by Tukey's multiple comparisons test, or Kruskal-Wallis tests followed by Dunn's multiple comparisons test.

Figure 8. Glial Gak/dAux contributes to PD pathology via regulating the V-ATPase assembly by a kinase-dependent switch The schematic diagram illustrating how Gak/dAux contributes to the underlying mechanisms of PD from a glial perspective. Lack of glial Gak/dAux induces a broad spectrum of parkinsonian symptoms in both flies and mice, including DA neurodegeneration, locomotor dysfunction, shorten lifespan, accumulation of pathological pS129-α-syn inclusions, and microglia activation. Mechanistically, dAux phosphorylates Vha44 at the serine 543 and affects the V-ATPase assembly, regulating lysosomal function and subsequent substrate degradation in glia.

References

1. Jellinger, K.A. (2018). Multiple System Atrophy: An Oligodendroglioneural Synucleinopathy1. J Alzheimers Dis *62*, 1141-1179. 10.3233/JAD-170397.
2. Peng, C., Trojanowski, J.Q., and Lee, V.M. (2020). Protein transmission in neurodegenerative disease. Nat Rev Neurol *16*, 199-212. 10.1038/s41582-020-0333-7.
3. Valdinocci, D., Radford, R.A., Siow, S.M., Chung, R.S., and Pountney, D.L.

(2017). Potential Modes of Intercellular alpha-Synuclein Transmission. Int J Mol Sci *18*. 10.3390/ijms18020469.

4. Tanriover, G., Bacioglu, M., Schweighauser, M., Mahler, J., Wegenast-Braun, B.M., Skodras, A., Obermuller, U., Barth, M., Kronenberg-Versteeg, D., Nilsson, K.P.R., et al. (2020). Prominent microglial inclusions in transgenic mouse models of alpha-synucleinopathy that are distinct from neuronal lesions. Acta Neuropathol Commun *8*, 133. 10.1186/s40478-020-00993-8.
5. Ho, M.S. (2019). Microglia in Parkinson's Disease. Adv Exp Med Biol *1175*, 335-353. 10.1007/978-981-13-9913-8_13.
6. Subhramanyam, C.S., Wang, C., Hu, Q., and Dheen, S.T. (2019). Microglia-mediated neuroinflammation in neurodegenerative diseases. Semin Cell Dev Biol *94*, 112-120. 10.1016/j.semcdb.2019.05.004.
7. Gleichman, A.J., and Carmichael, S.T. (2020). Glia in neurodegeneration: Drivers of disease or along for the ride? Neurobiol Dis *142*, 104957. 10.1016/j.nbd.2020.104957.
8. Cheng, J., Lu, Q., Song, L., and Ho, M.S. (2018). alpha-Synuclein Trafficking in Parkinson's Disease: Insights From Fly and Mouse Models. ASN Neuro *10*, 1759091418812587. 10.1177/1759091418812587.
9. Filippini, A., Gennarelli, M., and Russo, I. (2019). alpha-Synuclein and Glia in Parkinson's Disease: A Beneficial or a Detrimental Duet for the Endo-Lysosomal System? Cell Mol Neurobiol *39*, 161-168. 10.1007/s10571-019-00649-9.
10. Yi, S., Wang, L., Wang, H., Ho, M.S., and Zhang, S. (2022). Pathogenesis of alpha-Synuclein in Parkinson's Disease: From a Neuron-Glia Crosstalk Perspective. Int J Mol Sci *23*. 10.3390/ijms232314753.
11. Ballabio, A., and Bonifacino, J.S. (2020). Lysosomes as dynamic regulators of cell and organismal homeostasis. Nat Rev Mol Cell Biol *21*, 101-118. 10.1038/s41580-019-0185-4.
12. Paudel, R.R., Lu, D., Roy Chowdhury, S., Monroy, E.Y., and Wang, J. (2023). Targeted Protein Degradation via Lysosomes. Biochemistry *62*, 564-579. 10.1021/acs.biochem.2c00310.
13. Yang, C., and Wang, X. (2021). Lysosome biogenesis: Regulation and functions. J Cell Biol *220*. 10.1083/jcb.202102001.
14. Nishi, T., and Forgac, M. (2002). The vacuolar (H+)-ATPases--nature's most versatile proton pumps. Nat Rev Mol Cell Biol *3*, 94-103. 10.1038/nrm729.
15. Beyenbach, K.W., and Wieczorek, H. (2006). The V-type H+ ATPase: molecular structure and function, physiological roles and regulation. J Exp Biol *209*, 577-589. 10.1242/jeb.02014.
16. Stevens, T.H., and Forgac, M. (1997). Structure, function and regulation of the vacuolar (H+)-ATPase. Annu Rev Cell Dev Biol *13*, 779-808. 10.1146/annurev.cellbio.13.1.779.
17. Futai, M., Sun-Wada, G.H., Wada, Y., Matsumoto, N., and Nakanishi-Matsui,

M. (2019). Vacuolar-type ATPase: A proton pump to lysosomal trafficking. Proc Jpn Acad Ser B Phys Biol Sci *95*, 261-277. 10.2183/pjab.95.018.

18. Cotter, K., Stransky, L., McGuire, C., and Forgac, M. (2015). Recent Insights into the Structure, Regulation, and Function of the V-ATPases. Trends Biochem Sci *40*, 611-622. 10.1016/j.tibs.2015.08.005.

19. Song, Q., Meng, B., Xu, H., and Mao, Z. (2020). The emerging roles of vacuolar-type ATPase-dependent Lysosomal acidification in neurodegenerative diseases. Transl Neurodegener *9*, 17. 10.1186/s40035-020-00196-0.

20. Forgac, M. (2007). Vacuolar ATPases: rotary proton pumps in physiology and pathophysiology. Nat Rev Mol Cell Biol *8*, 917-929. 10.1038/nrm2272.

21. Zhang, S., Yi, S., Wang, L., Li, S., Wang, H., Song, L., Ou, J., Zhang, M., Wang, R., Wang, M., et al. (2023). Cyclin-G-associated kinase GAK/dAux regulates autophagy initiation via ULK1/Atg1 in glia. Proc Natl Acad Sci U S A *120*, e2301002120. 10.1073/pnas.2301002120.

22. Wang, L., Zhang, S., Yi, S., and Ho, M.S. (2023). A new regulator of autophagy initiation in glia. Autophagy, 1-3. 10.1080/15548627.2023.2251821.

23. Feany, M.B., and Bender, W.W. (2000). A Drosophila model of Parkinson's disease. Nature *404*, 394-398. 10.1038/35006074.

24. Miyazaki, M., Hiramoto, M., Takano, N., Kokuba, H., Takemura, J., Tokuhisa, M., Hino, H., Kazama, H., and Miyazawa, K. (2021). Targeted disruption of GAK stagnates autophagic flux by disturbing lysosomal dynamics. Int J Mol Med *48*. 10.3892/ijmm.2021.5028.

25. Munson, M.J., Mathai, B.J., Ng, M.Y.W., Trachsel-Moncho, L., de la Ballina, L.R., Schultz, S.W., Aman, Y., Lystad, A.H., Singh, S., Singh, S., et al. (2021). GAK and PRKCD are positive regulators of PRKN-independent mitophagy. Nat Commun *12*, 6101. 10.1038/s41467-021-26331-7.

26. Senturk, M., Lin, G., Zuo, Z., Mao, D., Watson, E., Mikos, A.G., and Bellen, H.J. (2019). Ubiquilins regulate autophagic flux through mTOR signalling and lysosomal acidification. Nat Cell Biol *21*, 384-396. 10.1038/s41556-019-0281-x.

27. Kovacs, A.L., Reith, A., and Seglen, P.O. (1982). Accumulation of autophagosomes after inhibition of hepatocytic protein degradation by vinblastine, leupeptin or a lysosomotropic amine. Exp Cell Res *137*, 191-201. 10.1016/0014-4827(82)90020-9.

28. Mauvezin, C., Nagy, P., Juhasz, G., and Neufeld, T.P. (2015). Autophagosome-lysosome fusion is independent of V-ATPase-mediated acidification. Nat Commun *6*, 7007. 10.1038/ncomms8007.

29. Bido, S., Muggeo, S., Massimino, L., Marzi, M.J., Giannelli, S.G., Melacini, E., Nannoni, M., Gambare, D., Bellini, E., Ordazzo, G., et al. (2021). Microglia-specific overexpression of alpha-synuclein leads to severe

dopaminergic neurodegeneration by phagocytic exhaustion and oxidative toxicity. Nat Commun *12*, 6237. 10.1038/s41467-021-26519-x.

30. Nabar, N.R., Heijjer, C.N., Shi, C.S., Hwang, I.Y., Ganesan, S., Karlsson, M.C.I., and Kehrl, J.H. (2022). LRRK2 is required for CD38-mediated NAADP-Ca(2+) signaling and the downstream activation of TFEB (transcription factor EB) in immune cells. Autophagy *18*, 204-222. 10.1080/15548627.2021.1954779.

31. Winslow, A.R., Chen, C.W., Corrochano, S., Acevedo-Arozena, A., Gordon, D.E., Peden, A.A., Lichtenberg, M., Menzies, F.M., Ravikumar, B., Imarisio, S., et al. (2010). alpha-Synuclein impairs macroautophagy: implications for Parkinson's disease. J Cell Biol *190*, 1023-1037. 10.1083/jcb.201003122.

32. Rivera, O.C., Hennigar, S.R., and Kelleher, S.L. (2018). ZnT2 is critical for lysosome acidification and biogenesis during mammary gland involution. Am J Physiol Regul Integr Comp Physiol *315*, R323-R335. 10.1152/ajpregu.00444.2017.

33. Kane, P.M. (1995). Disassembly and reassembly of the yeast vacuolar H(+)-ATPase in vivo. J Biol Chem *270*, 17025-17032.

34. Stransky, L.A., and Forgac, M. (2015). Amino Acid Availability Modulates Vacuolar H+-ATPase Assembly. J Biol Chem *290*, 27360-27369. 10.1074/jbc.M115.659128.

35. Sumner, J.P., Dow, J.A., Earley, F.G., Klein, U., Jager, D., and Wieczorek, H. (1995). Regulation of plasma membrane V-ATPase activity by dissociation of peripheral subunits. J Biol Chem *270*, 5649-5653. 10.1074/jbc.270.10.5649.

36. Zimmermann, B., Dames, P., Walz, B., and Baumann, O. (2003). Distribution and serotonin-induced activation of vacuolar-type H+-ATPase in the salivary glands of the blowfly Calliphora vicina. J Exp Biol *206*, 1867-1876. 10.1242/jeb.00376.

37. Trombetta, E.S., Ebersold, M., Garrett, W., Pypaert, M., and Mellman, I. (2003). Activation of lysosomal function during dendritic cell maturation. Science *299*, 1400-1403. 10.1126/science.1080106.

38. Myers, M., and Forgac, M. (1993). The coated vesicle vacuolar (H+)-ATPase associates with and is phosphorylated by the 50-kDa polypeptide of the clathrin assembly protein AP-2. J Biol Chem *268*, 9184-9186.

39. Alzamora, R., Thali, R.F., Gong, F., Smolak, C., Li, H., Baty, C.J., Bertrand, C.A., Auchli, Y., Brunisholz, R.A., Neumann, D., et al. (2010). PKA regulates vacuolar H+-ATPase localization and activity via direct phosphorylation of the a subunit in kidney cells. J Biol Chem *285*, 24676-24685. 10.1074/jbc.M110.106278.

40. Alzamora, R., Al-Bataineh, M.M., Liu, W., Gong, F., Li, H., Thali, R.F., Joho-Auchli, Y., Brunisholz, R.A., Satlin, L.M., Neumann, D., et al. (2013). AMP-activated protein kinase regulates the vacuolar H+-ATPase via direct phosphorylation of the A subunit (ATP6V1A) in the kidney. Am J Physiol

Renal Physiol *305*, F943-956. 10.1152/ajprenal.00303.2013.

41. Hong-Hermesdorf, A., Brux, A., Gruber, A., Gruber, G., and Schumacher, K. (2006). A WNK kinase binds and phosphorylates V-ATPase subunit C. FEBS Lett *580*, 932-939. 10.1016/j.febslet.2006.01.018.

42. Voss, M., Vitavska, O., Walz, B., Wieczorek, H., and Baumann, O. (2007). Stimulus-induced phosphorylation of vacuolar H(+)-ATPase by protein kinase A. J Biol Chem *282*, 33735-33742. 10.1074/jbc.M703368200.

43. Colacurcio, D.J., and Nixon, R.A. (2016). Disorders of lysosomal acidification-The emerging role of v-ATPase in aging and neurodegenerative disease. Ageing Res Rev *32*, 75-88. 10.1016/j.arr.2016.05.004.

44. Avrahami, L., Farfara, D., Shaham-Kol, M., Vassar, R., Frenkel, D., and Eldar-Finkelman, H. (2013). Inhibition of glycogen synthase kinase-3 ameliorates beta-amyloid pathology and restores lysosomal acidification and mammalian target of rapamycin activity in the Alzheimer disease mouse model: in vivo and in vitro studies. J Biol Chem *288*, 1295-1306. 10.1074/jbc.M112.409250.

45. Wallings, R., Connor-Robson, N., and Wade-Martins, R. (2019). LRRK2 interacts with the vacuolar-type H+-ATPase pump a1 subunit to regulate lysosomal function. Hum Mol Genet *28*, 2696-2710. 10.1093/hmg/ddz088.

46. Lee, J.H., Yu, W.H., Kumar, A., Lee, S., Mohan, P.S., Peterhoff, C.M., Wolfe, D.M., Martinez-Vicente, M., Massey, A.C., Sovak, G., et al. (2010). Lysosomal proteolysis and autophagy require presenilin 1 and are disrupted by Alzheimer-related PS1 mutations. Cell *141*, 1146-1158. 10.1016/j.cell.2010.05.008.

47. Im, E., Jiang, Y., Stavrides, P.H., Darji, S., Erdjument-Bromage, H., Neubert, T.A., Choi, J.Y., Wegiel, J., Lee, J.H., and Nixon, R.A. (2023). Lysosomal dysfunction in Down syndrome and Alzheimer mouse models is caused by v-ATPase inhibition by Tyr(682)-phosphorylated APP betaCTF. Sci Adv *9*, eadg1925. 10.1126/sciadv.adg1925.

48. Lin, C.H., Chen, M.L., Tai, Y.C., Yu, C.Y., and Wu, R.M. (2013). Reaffirmation of GAK, but not HLA-DRA, as a Parkinson's disease susceptibility gene in a Taiwanese population. Am J Med Genet B Neuropsychiatr Genet *162B*, 841-846. 10.1002/ajmg.b.32188.

49. Rhodes, S.L., Sinsheimer, J.S., Bordelon, Y., Bronstein, J.M., and Ritz, B. (2011). Replication of GWAS associations for GAK and MAPT in Parkinson's disease. Ann Hum Genet *75*, 195-200. 10.1111/j.1469-1809.2010.00616.x.

50. Tseng, W.E., Chen, C.M., Chen, Y.C., Yi, Z., Tan, E.K., and Wu, Y.R. (2013). Genetic variations of GAK in two Chinese Parkinson's disease populations: a case-control study. PLoS One *8*, e67506. 10.1371/journal.pone.0067506.

51. Beilina, A., Rudenko, I.N., Kaganovich, A., Civiero, L., Chau, H., Kalia, S.K., Kalia, L.V., Lobbestael, E., Chia, R., Ndukwe, K., et al. (2014). Unbiased screen for interactors of leucine-rich repeat kinase 2 supports a common

pathway for sporadic and familial Parkinson disease. Proc Natl Acad Sci U S A *111*, 2626-2631. 10.1073/pnas.1318306111.

52. Xu, Q., Bernardo, A., Walker, D., Kanegawa, T., Mahley, R.W., and Huang, Y. (2006). Profile and regulation of apolipoprotein E (ApoE) expression in the CNS in mice with targeting of green fluorescent protein gene to the ApoE locus. J Neurosci *26*, 4985-4994. 10.1523/JNEUROSCI.5476-05.2006.

53. Wang, L., Wang, H., Yi, S., Zhang, S., and Ho, M.S. (2022). A LRRK2/dLRRK-mediated lysosomal pathway that contributes to glial cell death and DA neuron survival. Traffic *23*, 506-520. 10.1111/tra.12866.

54. Yi, S., Wang, L., Ho, M.S., and Zhang, S. (2024). The autophagy protein Atg9 functions in glia and contributes to parkinsonian symptoms in a Drosophila model of Parkinson's disease. Neural Regen Res *19*, 1150-1155. 10.4103/1673-5374.382259.

55. Olsen, A.L., and Feany, M.B. (2019). Glial alpha-synuclein promotes neurodegeneration characterized by a distinct transcriptional program in vivo. Glia *67*, 1933-1957. 10.1002/glia.23671.

56. Olsen, A.L., and Feany, M.B. (2021). Parkinson's disease risk genes act in glia to control neuronal alpha-synuclein toxicity. Neurobiol Dis *159*, 105482. 10.1016/j.nbd.2021.105482.

Figure 1

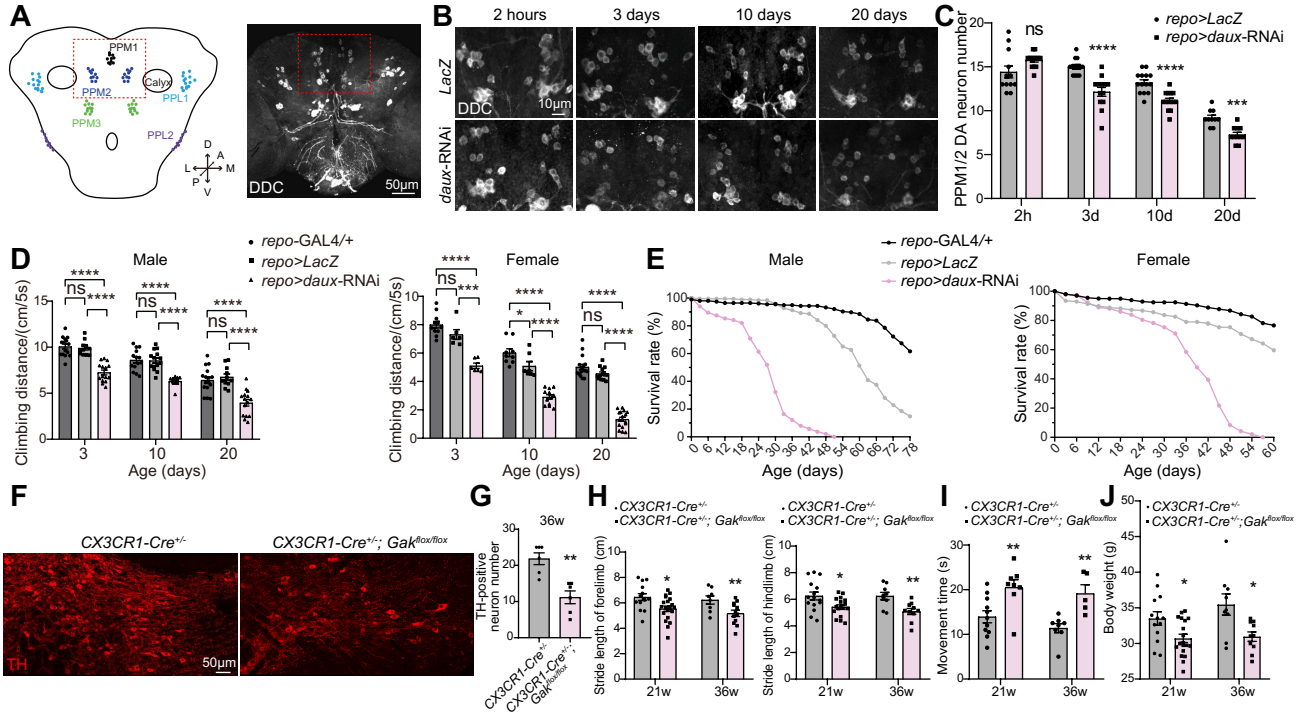
A
PPM1
PPM2
Calyx
PPL1
PPM3
PPL2
DDC
50μm
B
2 hours
3 days
10 days
20 days
LacZ
daux-RNAi
DDC
10μm
C
repo>LacZ
repo>daux-RNAi
PPM1/2 DA neuron number
ns
****
***
2h
3d
10d
20d
D
Male
Female
repo-GAL4/+
repo>LacZ
repo>daux-RNAi
Climbing distance/(cm/5s)
Age (days)
E
Male
Female
repo-GAL4/+
repo>LacZ
repo>daux-RNAi
Survival rate (%)
Age (days)
F
CX3CR1-Cre+/-
CX3CR1-Cre+/-; Gakflox/flox
TH
50μm
G
36w
TH-positive neuron number
H
CX3CR1-Cre+/-
CX3CR1-Cre+/-; Gakflox/flox
Stride length of forelimb (cm)
Stride length of hindlimb (cm)
21w
36w
I
Movement time (s)
J
Body weight (g)

Figure 2

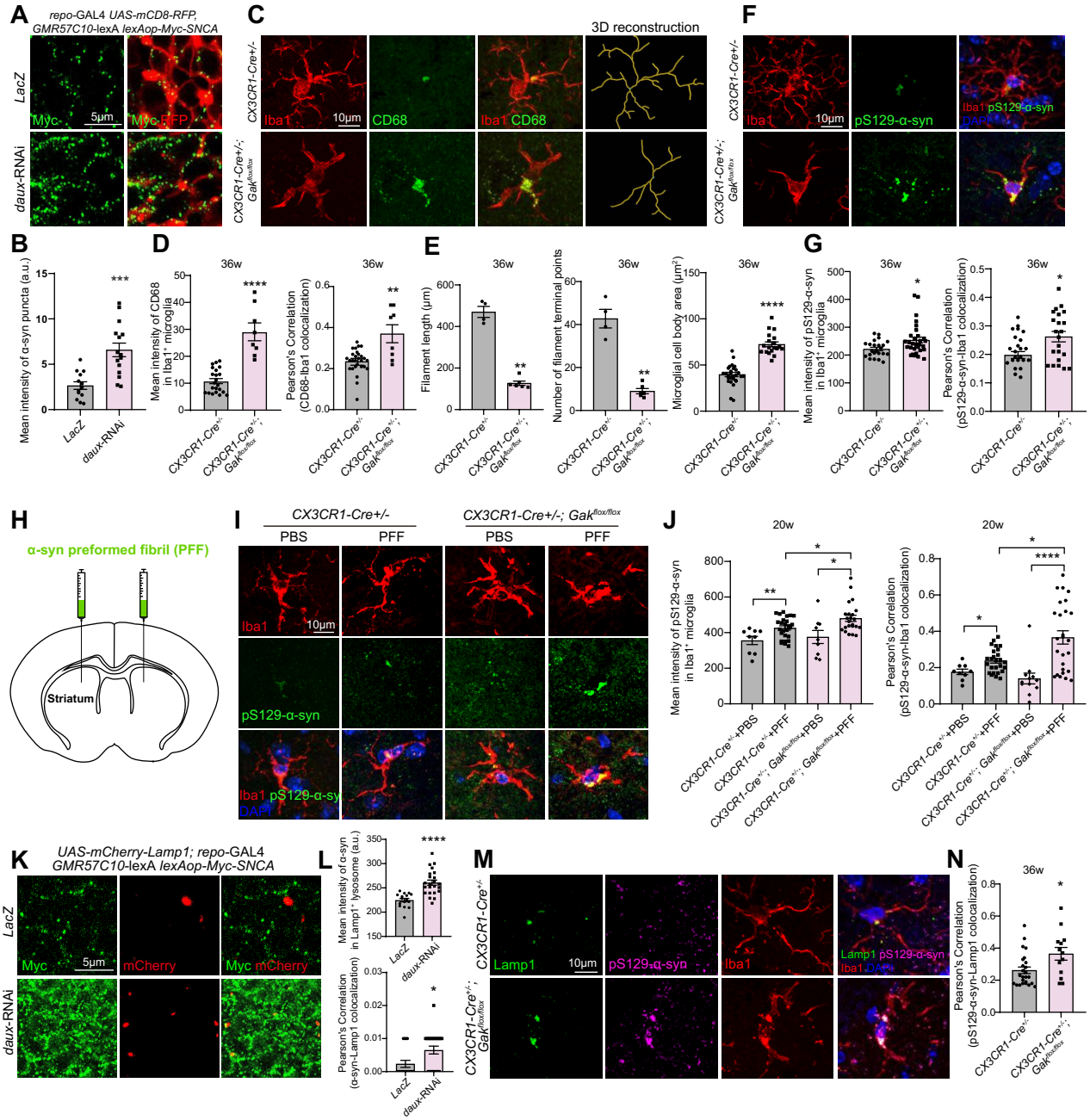
A
repo-GAL4 UAS-mCD8-RFP, GMR57C10-lexA lexAop-Myc-SNCA
LacZ
daux-RNAi
Myc
5μm
Myc RFP
B
Mean intensity of α-syn puncta (a.u.)
LacZ
daux-RNAi
C
3D reconstruction
CX3CR1-Cre+/-
CX3CR1-Cre+/-; Gakflox/flox
Iba1
10μm
CD68
Iba1 CD68
D
36w
Mean intensity of CD68 in Iba1+ microglia
Pearson's Correlation (CD68-Iba1 colocalization)
E
Filament length (μm)
Number of filament terminal points
Microglial cell body area (μm2)
F
pS129-α-syn
Iba1 pS129-α-syn DAPI
G
Mean intensity of pS129-α-syn in Iba1+ microglia
Pearson's Correlation (pS129-α-syn-Iba1 colocalization)
H
α-syn preformed fibril (PFF)
Striatum
I
CX3CR1-Cre+/-
CX3CR1-Cre+/-; Gakflox/flox
PBS
PFF
Iba1 pS129-α-syn DAPI
J
20w
Mean intensity of pS129-α-syn in Iba1+ microglia
Pearson's Correlation (pS129-α-syn-Iba1 colocalization)
CX3CR1-Cre+/-+PBS
CX3CR1-Cre+/-+PFF
CX3CR1-Cre+/-; Gakflox/flox+PBS
CX3CR1-Cre+/-; Gakflox/flox+PFF
K
UAS-mCherry-Lamp1; repo-GAL4 GMR57C10-lexA lexAop-Myc-SNCA
Myc
mCherry
Myc mCherry
L
Mean intensity of α-syn in Lamp1+ lysosome (a.u.)
Pearson's Correlation (α-syn-Lamp1 colocalization)
M
Lamp1
pS129-α-syn
Iba1
Lamp1 pS129-α-syn Iba1 DAPI
N
Pearson's Correlation (pS129-α-syn-Lamp1 colocalization)

Figure 3

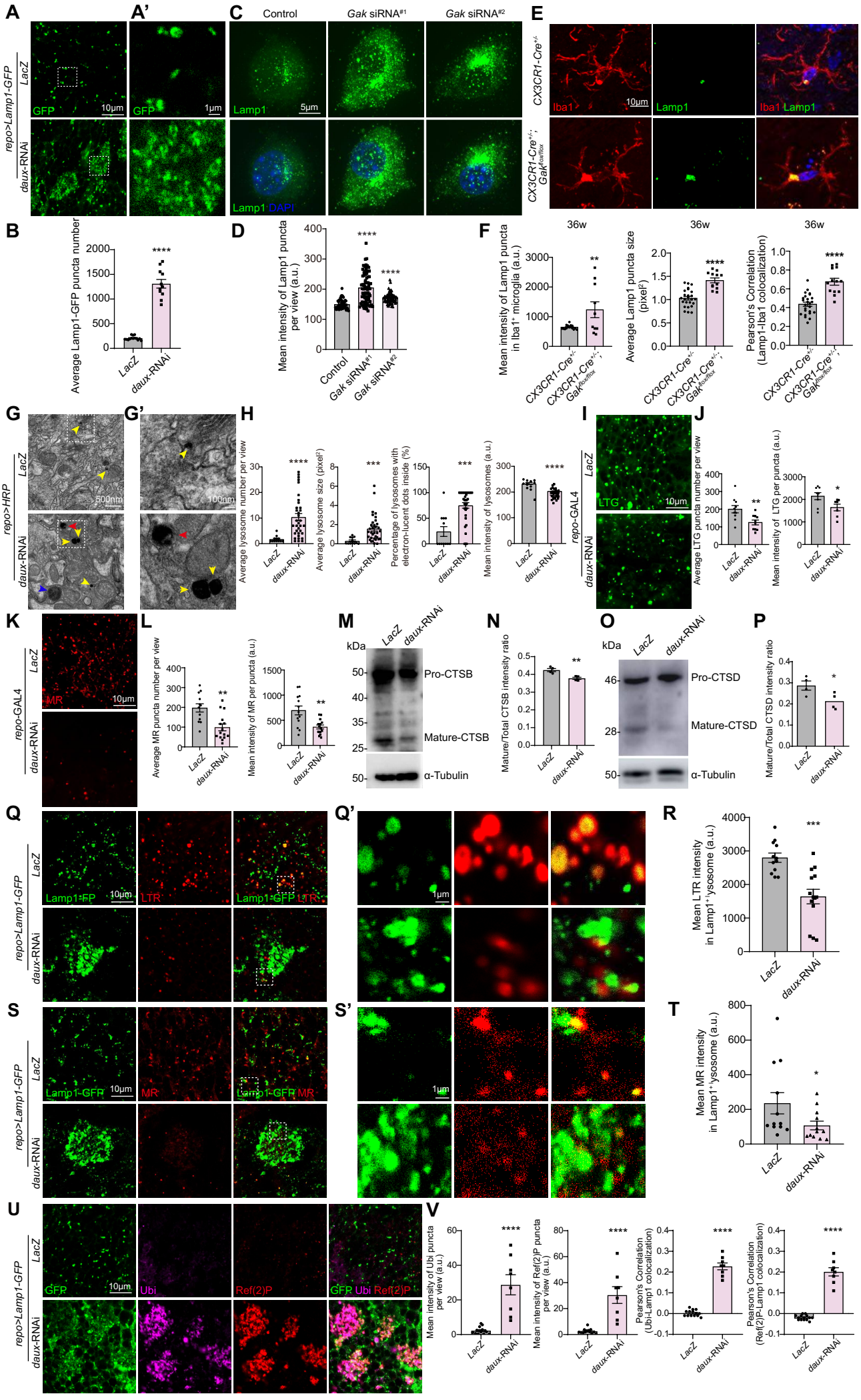
A
A'
C
Control
Gak siRNA#1
Gak siRNA#2
E
repo>Lamp1-GFP
LacZ
daux-RNAi
GFP
10μm
1μm
Lamp1
5μm
Lamp1 DAPI
CX3CR1-Cre+/-
CX3CR1-Cre+/-, Gakflox/flox
Iba1
Lamp1
Iba1 Lamp1
B
Average Lamp1-GFP puncta number
D
Mean intensity of Lamp1 puncta per view (a.u.)
F
36w
Mean intensity of Lamp1 puncta in Iba1+ microglia (a.u.)
Average Lamp1 puncta size (pixel²)
Pearson's Correlation (Lamp1-Iba1 colocalization)
G
G'
repo>HRP
500nm
100nm
H
Average lysosome number per view
Average lysosome size (pixel²)
Percentage of lysosomes with electron-lucent dots inside (%)
Mean intensity of lysosomes (a.u.)
I
repo-GAL4
LTG
J
Average LTG puncta number per view
Mean intensity of LTG per puncta (a.u.)
K
MR
L
Average MR puncta number per view
Mean intensity of MR per puncta (a.u.)
M
kDa
Pro-CTSB
Mature-CTSB
α-Tubulin
N
Mature/Total CTSB intensity ratio
O
Pro-CTSD
Mature-CTSD
P
Mature/Total CTSD intensity ratio
Q
Lamp1-FP
LTR
Lamp1-GFP LTR
Q'
R
Mean LTR intensity in Lamp1++ysosome (a.u.)
S
Lamp1-GFP
MR
Lamp1-GFP MR
S'
T
Mean MR intensity in Lamp1++ysosome (a.u.)
U
Ubi
Ref(2)P
GFP Ubi Ref(2)P
V
Mean intensity of Ubi puncta per view (a.u.)
Mean intensity of Ref(2)P puncta per view (a.u.)
Pearson's Correlation (Ubi-Lamp1 colocalization)
Pearson's Correlation (Ref(2)P-Lamp1 colocalization)

Figure 4

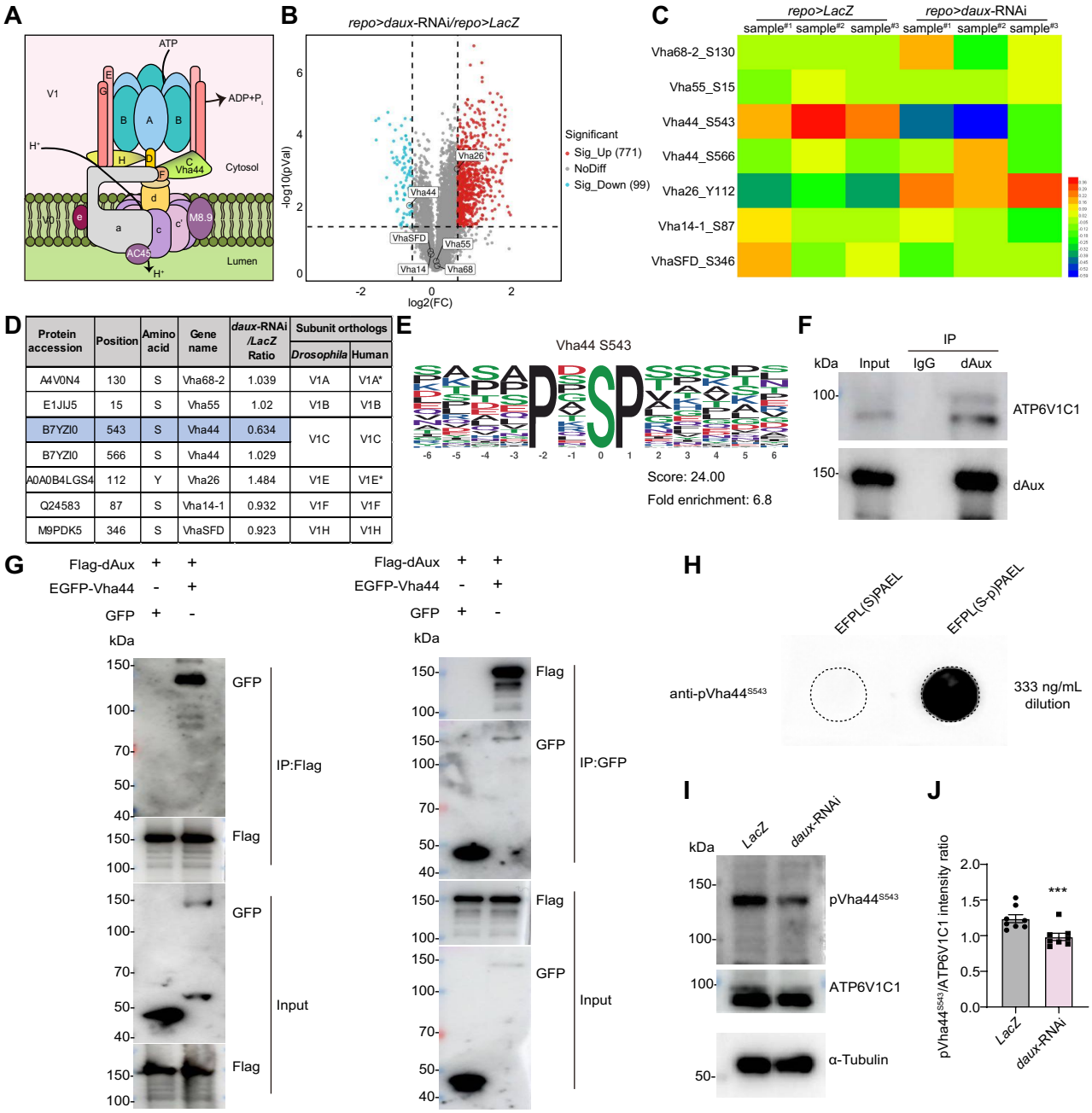

Protein accession	Position	Amino acid	Gene name	*daux*-RNAi /*LacZ* Ratio	Subunit orthologs	
					Drosophila	Human
A4V0N4	130	S	Vha68-2	1.039	V1A	V1A*
E1JIJ5	15	S	Vha55	1.02	V1B	V1B
B7YZI0	543	S	Vha44	0.634	V1C	V1C
B7YZI0	566	S	Vha44	1.029		
A0A0B4LGS4	112	Y	Vha26	1.484	V1E	V1E*
Q24583	87	S	Vha14-1	0.932	V1F	V1F
M9PDK5	346	S	VhaSFD	0.923	V1H	V1H

Figure 5

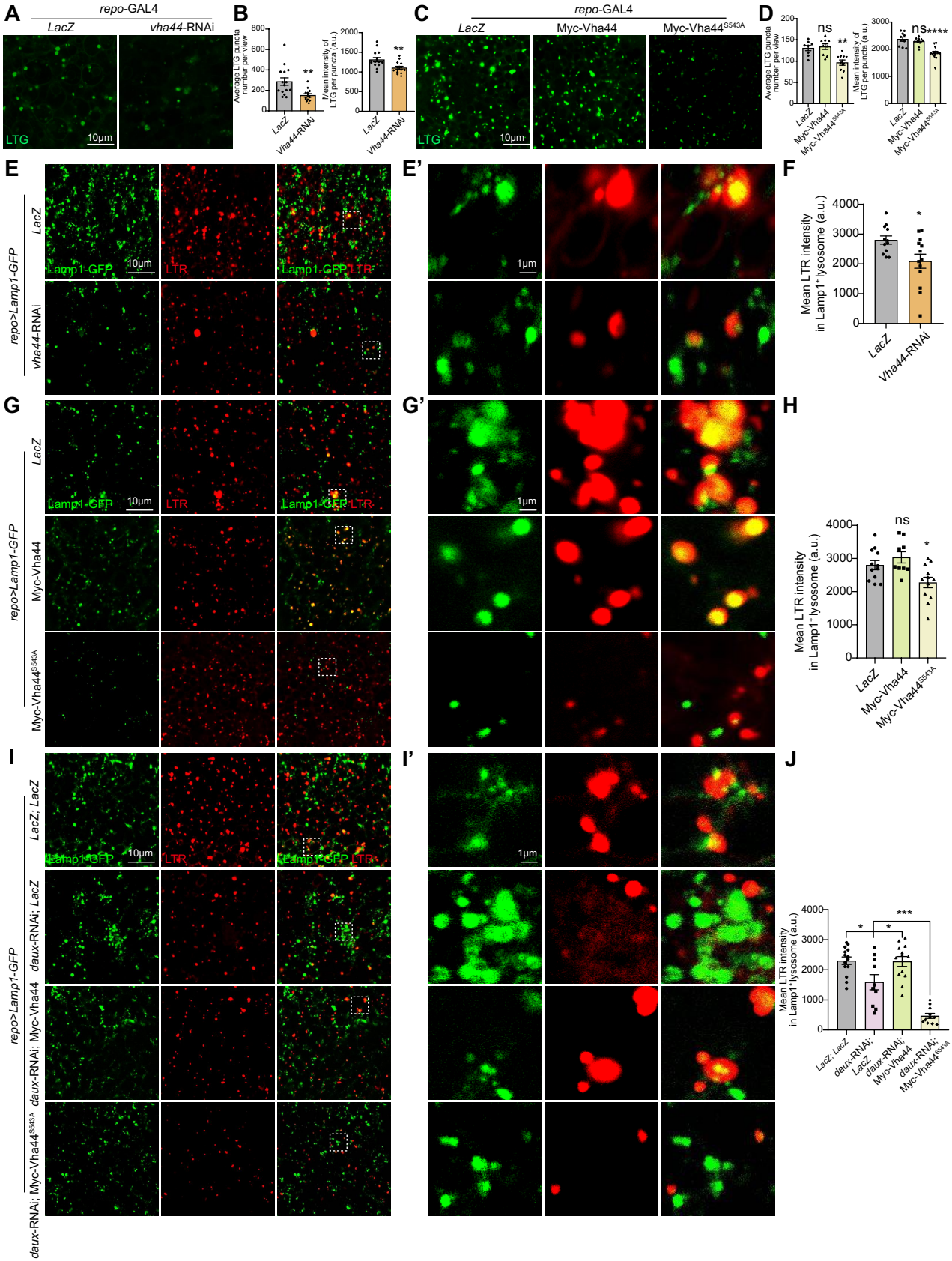

A
repo-GAL4
LacZ
vha44-RNAi
LTG
10μm
B
Average LTG puncta number per view
Mean intensity of LTG per puncta (a.u.)
LacZ
Vha44-RNAi
C
repo-GAL4
LacZ
Myc-Vha44
Myc-Vha44S543A
LTG
10μm
D
Average LTG puncta number per view
Mean intensity of LTG per puncta (a.u.)
ns
ns****
LacZ
Myc-Vha44
Myc-Vha44S543A
E
repo>Lamp1-GFP
LacZ
vha44-RNAi
Lamp1-GFP
LTR
Lamp1-GFP LTR
10μm
E'
1μm
F
Mean LTR intensity in Lamp1+ lysosome (a.u.)
LacZ
Vha44-RNAi
G
repo>Lamp1-GFP
LacZ
Myc-Vha44
Myc-Vha44S543A
Lamp1-GFP
LTR
Lamp1-GFP LTR
10μm
G'
1μm
H
Mean LTR intensity in Lamp1+ lysosome (a.u.)
ns
LacZ
Myc-Vha44
Myc-Vha44S543A
I
repo>Lamp1-GFP
LacZ; LacZ
daux-RNAi; LacZ
daux-RNAi; Myc-Vha44
daux-RNAi; Myc-Vha44S543A
Lamp1-GFP
LTR
Lamp1-GFP LTR
10μm
I'
1μm
J
Mean LTR intensity in Lamp1+ lysosome (a.u.)
LacZ; LacZ
daux-RNAi; LacZ
daux-RNAi; Myc-Vha44
daux-RNAi; Myc-Vha44S543A

Figure 6

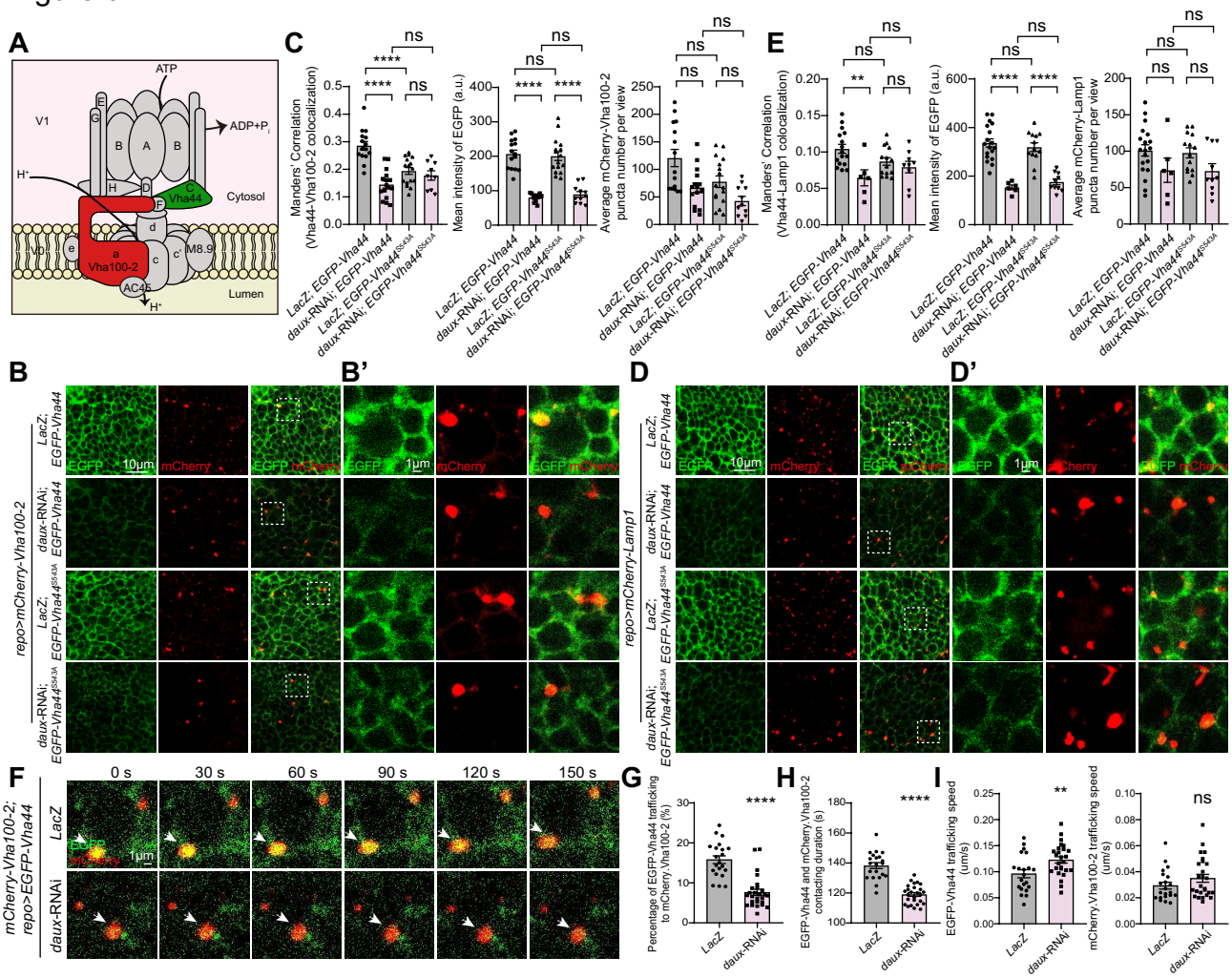
A
ATP
V1
ADP+Pi
H+
Vha44
Cytosol
Vha100-2
AC45
M8.9
Lumen
B
B'
D
D'
repo>mCherry-Vha100-2
repo>mCherry-Lamp1
LacZ; EGFP-Vha44
daux-RNAi; EGFP-Vha44
LacZ; EGFP-Vha44S543A
daux-RNAi; EGFP-Vha44S543A
EGFP
mCherry
10μm
1μm
C
Manders' Correlation (Vha44-Vha100-2 colocalization)
Mean intensity of EGFP (a.u.)
Average mCherry-Vha100-2 puncta number per view
E
Manders' Correlation (Vha44-Lamp1 colocalization)
Mean intensity of EGFP (a.u.)
Average mCherry-Lamp1 puncta number per view
LacZ; EGFP-Vha44
daux-RNAi; EGFP-Vha44
LacZ; EGFP-Vha44S543A
daux-RNAi; EGFP-Vha44S543A
ns
****
**
F
0 s
30 s
60 s
90 s
120 s
150 s
mCherry-Vha100-2; repo>EGFP-Vha44
LacZ
daux-RNAi
G
Percentage of EGFP-Vha44 trafficking to mCherry-Vha100-2 (%)
H
EGFP-Vha44 and mCherry-Vha100-2 contacting duration (s)
I
EGFP-Vha44 trafficking speed (um/s)
mCherry-Vha100-2 trafficking speed (um/s)
LacZ
daux-RNAi

Figure 7

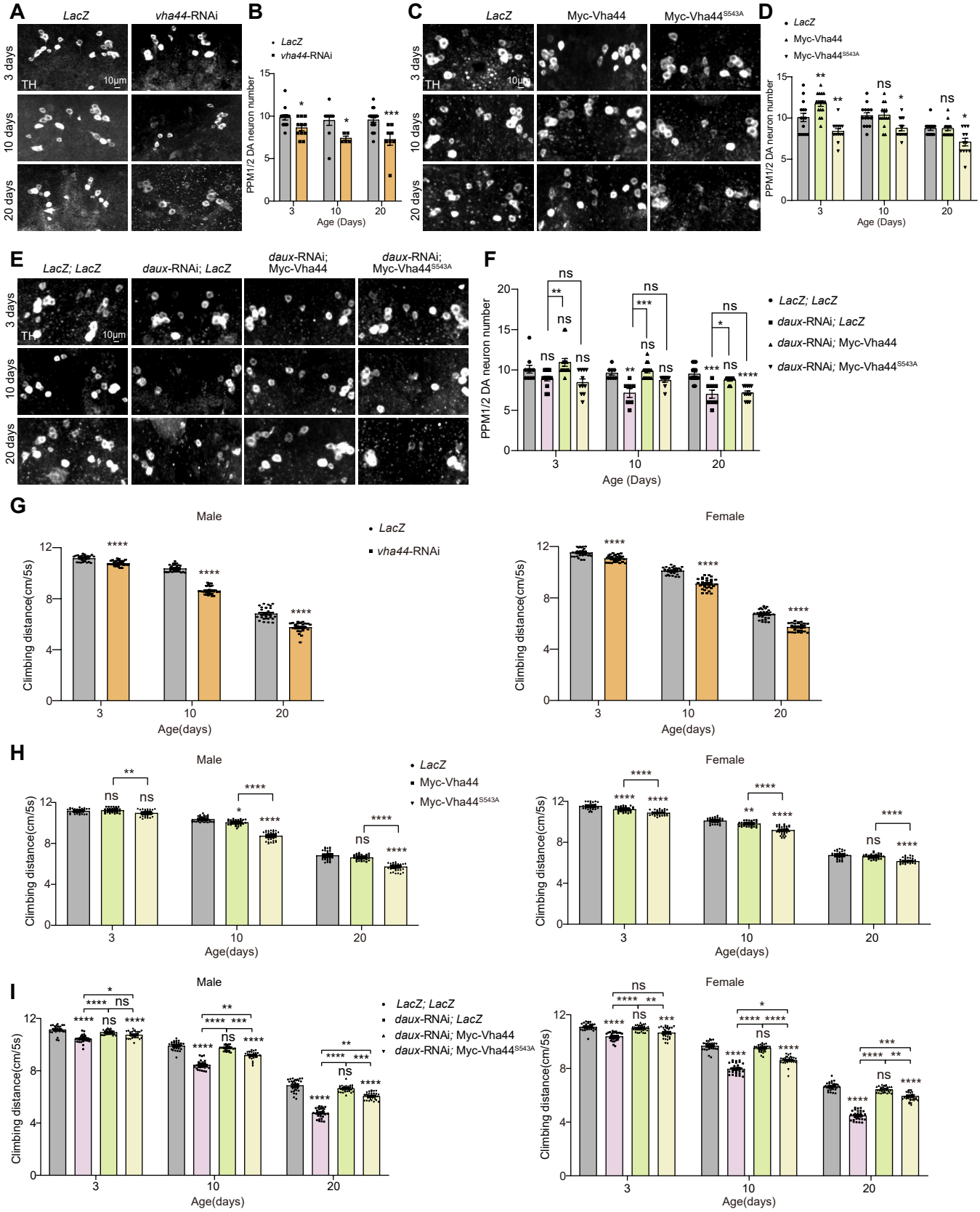
A
LacZ
vha44-RNAi
3 days
10 days
20 days
TH
10μm
B
LacZ
vha44-RNAi
PPM1/2 DA neuron number
Age (Days)
C
LacZ
Myc-Vha44
Myc-Vha44S543A
D
LacZ
Myc-Vha44
Myc-Vha44S543A
E
LacZ; LacZ
daux-RNAi; LacZ
daux-RNAi; Myc-Vha44
daux-RNAi; Myc-Vha44S543A
F
LacZ; LacZ
daux-RNAi; LacZ
daux-RNAi; Myc-Vha44
daux-RNAi; Myc-Vha44S543A
G
Male
Female
LacZ
vha44-RNAi
Climbing distance(cm/5s)
Age(days)
H
Male
Female
LacZ
Myc-Vha44
Myc-Vha44S543A
I
Male
Female
LacZ; LacZ
daux-RNAi; LacZ
daux-RNAi; Myc-Vha44
daux-RNAi; Myc-Vha44S543A

Figure 8

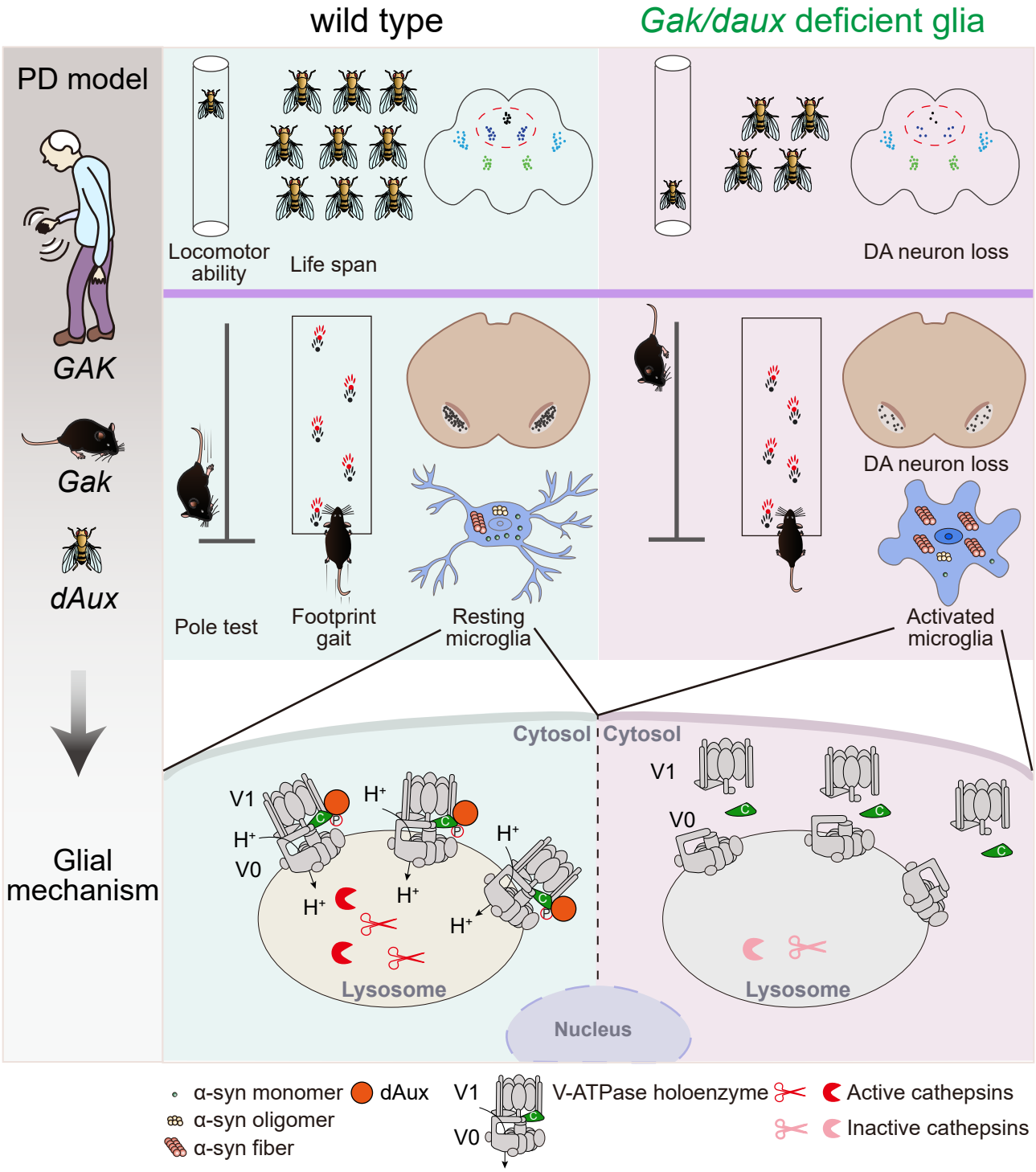
wild type
Gak/daux deficient glia
PD model
GAK
Gak
dAux
Locomotor ability
Life span
DA neuron loss
Pole test
Footprint gait
Resting microglia
DA neuron loss
Activated microglia
Glial mechanism
Cytosol
Cytosol
V1
V0
H+
Lysosome
Lysosome
Nucleus
α-syn monomer
α-syn oligomer
α-syn fiber
dAux
V-ATPase holoenzyme
Active cathepsins
Inactive cathepsins